Batteries Hot Paper

International Edition: DOI: 10.1002/anie.201909805
German Edition: DOI: 10.1002/ange.201909805

# Water-Mediated Synthesis of a Superionic Halide Solid Electrolyte

*Xiaona Li[+], Jianwen Liang[+], Ning Chen, Jing Luo, Keegan R. Adair, Changhong Wang, Mohammad Norouzi Banis, Tsun-Kong Sham, Li Zhang, Shangqian Zhao, Shigang Lu, Huan Huang, Ruying Li, and Xueliang Sun**

**Abstract:** *To promote the development of solid-state batteries, polymer-, oxide-, and sulfide-based solid-state electrolytes (SSEs) have been extensively investigated. However, the disadvantages of these SSEs, such as high-temperature sintering of oxides, air instability of sulfides, and narrow electrochemical windows of polymers electrolytes, significantly hinder their practical application. Therefore, developing SSEs that have a high ionic conductivity ($>10^{-3}$ S cm$^{-1}$), good air stability, wide electrochemical window, excellent electrode interface stability, low-cost mass production is required. Herein we report a halide $Li^+$ superionic conductor, $Li_3InCl_6$, that can be synthesized in water. Most importantly, the as-synthesized $Li_3InCl_6$ shows a high ionic conductivity of $2.04\times10^{-3}$ S cm$^{-1}$ at 25 °C. Furthermore, the ionic conductivity can be recovered after dissolution in water. Combined with a $LiNi_{0.8}Co_{0.1}Mn_{0.1}O_2$ cathode, the solid-state Li battery shows good cycling stability.*

All-solid-state lithium batteries (ASSLBs) using solid-state electrolytes (SSEs) are considered as promising next-generation energy-storage systems with improved safety through the elimination of the flammable liquid electrolyte in convention lithium-ion batteries (LIBs).[1] Among the various types of electrolytes, oxide-based and sulfide-based SSEs are considered to be the most promising candidates for use in ASSLBs because of their high ionic conductivity of over $10^{-3}$ S cm$^{-1}$.[1c,2] Despite the recent progress made in these SSEs, several serious obstacles are still hindering their practical applications, especially the manufacturing complexity and sensitivity.[3]

For oxide-based SSEs, high sintering temperatures are required both during the synthesis of SSEs and in the subsequent steps to promote intimate contact between electrode materials and SSE, making the manufacturing costly and which also might cause interfacial reactions.[4] For sulfide-based SSEs, their chemical instability in air and moisture inevitably cause deterioration of the structure/composition, leading to a large decrease in ionic conductivity and the release of noxious $H_2S$ gas.[5] Another serious challenge for sulfide SSEs is the unavoidable and detrimental side reactions with high-voltage oxide cathode materials (e.g. $LiCoO_2$ and $LiNi_xMn_yCo_zO_2$).[6] Direct contact between sulfide SSEs and oxide cathode materials results in the formation of a lithium deficient space-charge layer and the diffusion of transition metals from cathode to sulfide SSE which react with the electrolyte and form metal sulfides.[7] In this context, interfacial protection layers between sulfide SSEs and oxide cathodes are necessary but introduce extra complexity and cost for the fabrication process.[6b,8]

To address these issues, halide SSEs, which were developed in the 1970s, have emerged as attractive alternatives.[9] Unfortunately, the development of halide SSEs has been limited due to their relatively low ionic conductivity and the structural instability of some species.[1d,10] For example, the $Li_3YCl_6$ synthesized by Lutz and Steiner in 1992 only achieved an ionic conductivity of approximately $10^{-4}$ S cm$^{-1}$ at 200 °C.[9a] Although high-temperature phase $Li_3InBr_6$ has a high ionic conductivity of $10^{-3}$ S cm$^{-1}$ at 25 °C, the as-prepared $Li_3InBr_6$ shows quite low ionic conductivity of $10^{-7}$ S cm$^{-1}$ and its structure will be destroyed at −13 °C.[11] In more recent times, the relatively stable $Li_3YCl_6$ and $Li_3YBr_6$ SSEs with high ionic conductivities of around $10^{-3}$ S cm$^{-1}$ were synthesized by Asano et al. using a high-energy ball milling and high-temperature annealing process.[12] Nevertheless, these $Li^+$-conducting halide SSEs are still sensitive to moisture.[10,13]

Achieving high ionic conductivity, high stability toward oxide cathodes, moisture resistance, and a water-based synthesis method would be an ultimate goal for halide SSEs. Herein, we report a halide-based SSE, $Li_3InCl_6$, that can be synthesized via a $H_2O$-mediated route (see Equation (1)). The reaction between LiCl and $InCl_3$ can be mediated by $H_2O$ at room temperature to form $Li_3InCl_6{\cdot}xH_2O$, and the removal of $H_2O$ affords pure $Li_3InCl_6$ and recovered conductivity (Figure 1). The $Li_3InCl_6$ SSE possesses a high ionic conduc-

[*] Dr. X. Li,[+] Dr. J. Liang,[+] J. Luo, K. R. Adair, C. Wang, Dr. M. N. Banis, Dr. R. Li, Prof. X. Sun
Department of Mechanical and Materials Engineering
University of Western Ontario
1151 Richmond St, London, Ontario, N6A 3K7 (Canada)
E-mail: xsun9@uwo.ca
Dr. N. Chen, Dr. M. N. Banis
Canadian Light Source
44 Innovation Boulevard, Saskatoon, SK S7N 2V3 (Canada)
Prof. T. Sham
Department of Chemistry, University of Western Ontario
1151 Richmond St, London, Ontario, N6A 3K7 (Canada)
Dr. L. Zhang, Dr. S. Zhao, Dr. S. Lu
China Automotive Battery Research Institute Co. Ltd.
5th Floor, No. 43, Mining Building
North Sanhuan Middle Road, Beijing, 100088 (China)
Dr. H. Huang
Glabat Solid-State Battery Inc.
700 Collip Circle, London, ON, N6G 4X8 (Canada)
[+] These authors contributed equally to this work.
Supporting information and the ORCID identification number(s) for the author(s) of this article can be found under: https://doi.org/10.1002/anie.201909805.

  

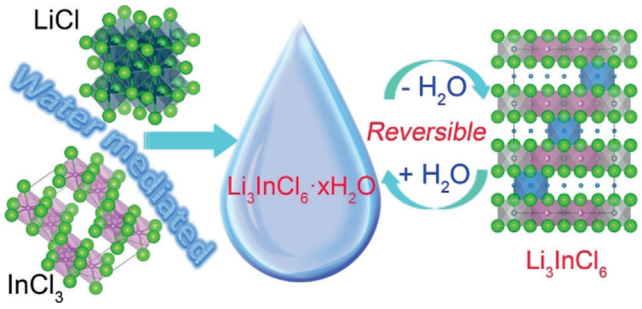


***Figure 1.*** Illustration of water-mediated synthesis route for $Li_3InCl_6$ SSE and the reversible interconversion between the hydrated a $Li_3InCl_6{\cdot}x\,H_2O$ and dehydrated $Li_3InCl_6$. Green Cl, purple In, blue Li.

tivity of $2.04\times10^{-3}$ S cm$^{-1}$ at 25 °C and good chemical/electrochemical stability toward traditional oxide cathodes. This halide SSE delivered essential advantages over commercial sulfide-SSEs in terms of synthetic simplicity, air/humidity stability, and direct compatibility (both chemically and electrochemically) with oxide cathodes. Excellent electrochemical performance is demonstrated in ASSLBs assembled with $LiNi_{0.8}Mn_{0.1}Co_{0.1}O_2$ (NMC811) cathode.

$Li_3InCl_6$ SSE was synthesized from a $H_2O$-mediated route from precursors in water [Eq. (1)]. Typically, commercial LiCl and $InCl_3$ precursors with a molar ratio of 3:1 were dissolved in water. After evaporation of the water, the product was highly crystalline as shown in Figure S1 in the Supporting Information. The corresponding X-ray diffraction (XRD) patterns were not matched to any particular chemicals including LiCl, $InCl_3$, $InCl_3{\cdot}x\,H_2O$, and $Li_3InCl_6$. The obtained product was probably a hydrated form of lithium indium chloride as $Li_3InCl_6{\cdot}x\,H_2O$ similar to other indium halide hydrates, such as $Cs_2InBr_5{\cdot}H_2O$,[14] $(NH_4)_2InCl_5{\cdot}H_2O$[15] and $K_3InCl_6{\cdot}n\,H_2O$.[15] Coordinating water was confirmed by Fourier transform infrared spectroscopy (Figure S2). The number of coordinated water ($x$ in $Li_3InCl_6{\cdot}x\,H_2O$) was estimated to be 2 by thermogravimetric analysis (TGA, Figure S3). Different dehydration temperatures from 100 to 200 °C were chosen for post-treatment based on the TGA curves.

$$3\,LiCl + InCl_3 \xrightarrow{H_2O} Li_3InCl_6\cdot x\,H_2O \xrightarrow{\Delta} Li_3InCl_6 \qquad (1)$$

After heating the $Li_3InCl_6{\cdot}2\,H_2O$ under vacuum at 200 °C for 4 h, the dehydrated sample was obtained. The corresponding XRD pattern shown in Figure S4 can be indexed to $Li_3InCl_6$. The XRD patterns of other samples obtained from dehydration attempts at lower vacuum temperatures of 100 and 130 °C are shown in Figure S5. The dehydrated form of $Li_3InCl_6$ can also be obtained through a dehydration process in air or Ar, while an impurity phase of InOCl appeared (Figure S6, S7). Thus, the dehydration process was conducted under vacuum to ensure high purity. From an energy sustainable and ease of handling point of view, the facile aqueous synthetic route for $Li_3InCl_6$ is extremely attractive compared to the conventional high-energy and expensive ball-milling and high temperature annealing process required for other SSEs.[12]

The ionic conductivity of the $Li_3InCl_6$ SSE obtained at 200 °C was studied by electrochemical impedance spectroscopy (Figure 2a). The plotted ionic conductivities were calculated from the sum of the grain boundary and bulk

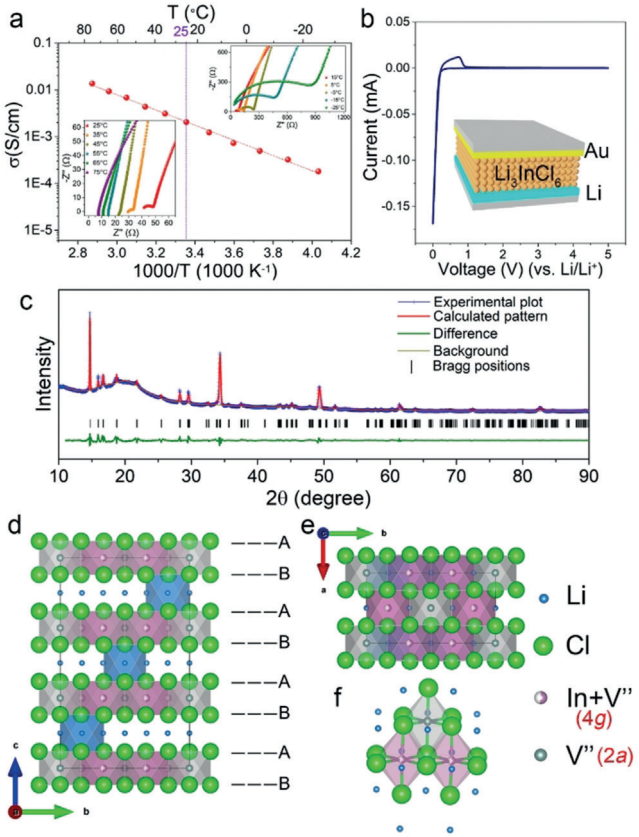


***Figure 2.*** a) Impedance plots of the conductivity data from low to high temperatures (insets) and Arrhenius conductivity plots of $Li_3InCl_6$ SSEs. b) Cyclic voltammogram of Li/$Li_3InCl_6$/Au cell versus Li/$Li^+$ from 0 to 5.0 V at a scan rate of 0.1 mV s$^{-1}$. Inset: schematic representation of the cell. c) Representative powder X-ray diffraction pattern of $Li_3InCl_6$ and the corresponding Rietveld refinements. Structure of $Li_3InCl_6$: d),e) Layered structure observed from the view of perpendicular to *a*-axis, $Li^+$ (blue), $In^{3+}$ (purple) and vacancy (V", grey); $Cl^-$ (green balls). f) Typical $Li^+$ location around the $InCl_6^{3-}$ octahedron.

resistance featured with a semicircle in the high frequency region as presented in the inset of Figure 2a. The ionic conductivity of $Li_3InCl_6$ is $2.04\times10^{-3}$ S cm$^{-1}$ at 25 °C, which is among the best reported halide SSEs.[9a,10,12,16] The corresponding activation energy ($E_a$) calculated based on the Arrhenius equation[1d] is 0.347 eV. The electronic conductivity ($\sigma_{dc\text{-}electron}$) of $Li_3InCl_6$ was determined to be $1.86\times10^{-9}$ S cm$^{-1}$ by a direct current (DC) polarization measurement[17] (Figure S8). The low value of electronic conductivity compared to the ionic contribution makes it good SSE candidate for practical application.[18] The electrochemical stability of the $Li_3InCl_6$ SSE was evaluated by cyclic voltammetry (CV) with a Li/$Li_3InCl_6$/Au cell at 25 °C (Figure 2b). The cell displayed reversible cathodic and anodic current response around 0 V, which is similar to other SSEs reported previously,[2a] and further indicated that $Li_3InCl_6$ is not stable towards Li metal.

  

Favorably, the absence of oxidation currents at high voltages indicated a practical electrochemical stability.[19] The ionic conductivities and activation energies of $Li_3InCl_6$ SSEs obtained at 100 and 130 °C under vacuum are also compared in Figure S9 and Table S1. Clearly, the ionic conductivity of the $Li_3InCl_6$ obtained at 200 °C is at its highest. Moreover, the synthesis of $Li_3InCl_6$ SSEs can be easily scaled-up to 110 g through the $H_2O$-mediated synthesis route with high purity and ionic conductivity ($1.54 \times 10^{-3}$ S cm$^{-1}$ at 25 °C) as shown in Figure S10.

Figure 2c presents a slow scan powder XRD and crystal structure with Rietveld refinement of the $Li_3InCl_6$ sample that belongs to monoclinic symmetry (space group *C*2/*m*). The structure was refined using the Rietveld method combined with the DFT Geometry Optimization calculation.[20] Table S2, S3 shows the detailed structural information of the Rietveld refinement results, which reveal a different structure to that of $Li_3InCl_6$ in the database (ICSD No. 04-009-9027, Table S4). The distorted rock-salt structure of $Li_3InCl_6$ (Figure 2d–f) exhibits an AB AB $Cl^-$ packing with both $Li^+$ and $In^{3+}$ ions in the octahedral sites ($LiCl_6$ and $InCl_6$ octahedra) and vacancies in two independents octahedral sites (V"$Cl_6$ octahedron, V" is vacancy). The vacancy in the 4*g* site (V"$_{4g}$) is shared with $In^{3+}$ and the vacancy occupation is around 47 %. In contrast, the vacancy of the 2*a* site (V"$_{2a}$) shows 100 % occupation. From the symmetry and electrostatic point of view, the V"$_{2a}$ site is expected to be more stable than the site of V"$_{4g}$. Meanwhile, DFT calculation further confirms the lower energy in the vacancy formation of V"$_{2a}$ than V"$_{4g}$. Thus, the vacancy distribution within the synthesized $Li_3InCl_6$ is quite different from that of the database, indicating that different $Li^+$ conduction and migration properties may be present since those vacancies are highly related to the ionic conductivity.[21]

Furthermore, indium *K*-edge X-ray absorption fine structure (XAFS) was employed to further reveal the detailed structure of the $Li_3InCl_6$. The XAFS model M-1 (the first model) was developed based on the crystallographic structure of $Li_3InCl_6$ in the database, theoretical modeling and further verified by the Rietveld refinement upon XRD of the synthesized $Li_3InCl_6$ (Figure 3a–d). The shell by shell local structural around the indium center of the original structural model was divided into a three shells model, incorporating backscattering from neighboring atoms with an interatomic distance up to around 5.0 Å, which is roughly equivalent to the typical EXAFS detection limit (Table S5). A Gaussian window function was used for Fourier transform (FT) during fitting (detailed information shown in supporting information).[22] The Feff R space fitting result is compared to the experimental data, revealing an overall matching in both magnitude and imaginary part of the FT with certain fitting for the R region shorter than approximately 1.4 Å (Figure 3b), which is also proved by the comparison of *k* space for $k^2\chi(k)$ results (Figure S11). Moreover, the fitted structural parameters (Table S5) are consistent well with the indium local structural environment predicted by crystallography.

The M-2 (the second model) structural system was developed based on the same crystallography data of $Li_3InCl_6$ used for developing M-1. The radius of the indium

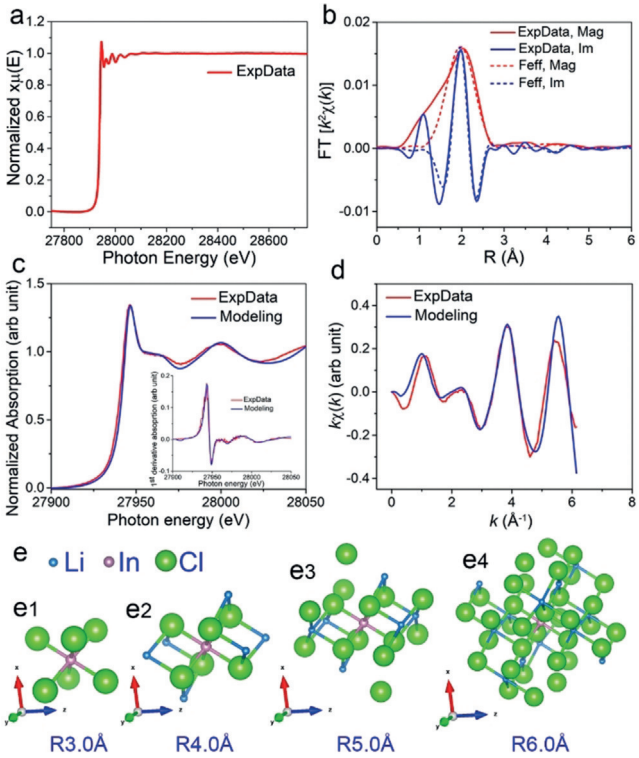


***Figure 3.*** a) XAS spectra of $Li_3InCl_6$. b) R space curve fitting result, showing the experimental data (red solid) and Feff modeling (red dash) in terms of magnitude of FT and the imaginary part of FT (experimental data (blue solid) and Feff modeling (blue dash) traces). The comparison between XANES modeling and experimental data in c) XANES spectra (inset: corresponding first derivative spectra), and d) for $k\chi(k)$. e1)–e4) The XAFS model M-2 structural system based on the crystallography of $Li_3InCl_6$ after DFT calculation and X-ray refinement. The system is composed of In centered spherical clusters with the radius progressively increasing from 3.0 Å to 6.0 Å.

centered clusters is progressively increased from the first shell $InCl_6$ octahedron (i.e., R3.0 Å, Figure 3e1) to R6.0 Å cluster (Figure 3e4), matching the usual XAFS detection capability. The M-2 based theoretical X-ray absorption near edge structure (XANES) spectrum and corresponding first derivative spectrum system are shown in Figure S12. Based on features "A" and "B", the XANES modeling best-fit was obtained based on the cluster R5.0 Å (Figure 3e3). The comparison is made correspondingly among the best-fit versus the experimental data in XANES (Figure 3c), first derivative spectrum (Figure 3c insert), and $k\chi(k)$ (Figure 3d), revealing close agreement between them. This result clearly indicates that the indium local structure environment of the synthesized $Li_3InCl_6$ SSE is consistent with the result from the DFT theoretical modeling and the XRD Rietveld refinement. The observed particle size of synthesized $Li_3InCl_6$ SSE (Figure S13) is around several hundreds of nanometers, which consists of aggregates of small $Li_3InCl_6$ particles.

Given that the $Li_3InCl_6$ SSE can be synthesized through an $H_2O$-mediated synthesis route directly, we intentionally expose the $Li_3InCl_6$ SSE to humidity to investigate its stability and recoverability. The influence of humidity was studied by completely dissolving $Li_3InCl_6$ in deionized water. The pH

  

value of $Li_3InCl_6$ solution (10 wt%) is about 5, which is similar to the solution of the precursors ($LiCl + InCl_3$, 10 wt%) as shown in Figure S14, S15. The retrieved sample after dissolution in water and drying exhibited a similar XRD pattern to the hydrated form of $Li_3InCl_6{\cdot}2H_2O$ (Figure S16). After heating/dehydration at 200 °C for 1 h under vacuum, the "spoiled" sample was able to fully recover the pristine $Li_3InCl_6$ structure according to XRD and X-ray photoelectron spectroscopy (XPS) results (Figure 4a, Figure S17). The corresponding ionic conductivity and activation energy of the recovered sample were observed to be $1.88 \times 10^{-3}$ S cm$^{-1}$ (25 °C) and 0.351 eV (Figure 4b), respectively. It can be concluded that, no significant changes in ionic conductivity or activation energy were observed, demonstrating that $Li_3InCl_6$ SSE has good humidity stability with recoverable superionic conductivity. The ionic conductivity and structure evolution of $Li_3InCl_6$ SSE exposed to different humidity of 3–5% and 30% without reheating process were further measured. The ionic conductivity of $Li_3InCl_6$ SSEs can still achieve over $10^{-3}$ S cm$^{-1}$ and $10^{-4}$ S cm$^{-1}$ for 7.5 h and 24 h exposure time in 3–5% humidity, respectively (Figure 4c,d). Even after 24 h exposure, the main XRD patterns can be indexed to pristine $Li_3InCl_6$ as shown in Figure S18. When increase the humidity to 30%, the conductivity of exposed $Li_3InCl_6$ reduced a lot along exposure time, with $3.98 \times 10^{-7}$ S cm$^{-1}$ achieved after 24 h (Figure 4d, S19), which is caused by the easier formation of $Li_3InCl_6{\cdot}2H_2O$ (Figure S20). No other oxidized or hydrolyzed species were observed as supported by XPS results (Figure S21, S22). Both the samples reheated again still recover back to $Li_3InCl_6$ (Figure S18, S20). The results proved that the dehydration/hydration process between $Li_3InCl_6{\cdot}2H_2O$ and $Li_3InCl_6$ is reversible under certain conditions.

The $Li_3InCl_6$ electrolyte was evaluated as a solid electrolyte for practical ASSLBs. Figure 5a shows the charge–discharge curves of the assembled ASSLBs using NMC811/$Li_3InCl_6$ as the cathode (SEM and energy dispersive X-ray mapping images shown in Figure S23), $Li_3InCl_6$ as the electrolyte, and In as the anode between of 1.9–3.8 V versus LiIn/$Li^+$ at 0.13 mA cm$^{-2}$ (25 °C, with active NMC811 loading of 8.92 mg cm$^{-2}$). A thin $Li_{10}GeP_2S_{12}$ layer was set between $Li_3InCl_6$ and In anode. The ASSLB exhibited a reversible capacity over 154 mAh g$^{-1}$. A high initial Coulombic Efficiency of 84.2% was achieved, which is among the best reported for NMC811 cathodes in ASSLBs.[1c,7a,8,23] Stable cycling performance was achieved for 70 cycles, with a reversible capacity of 150 mAh g$^{-1}$ maintained. Good rate capability was also demonstrated as shown in Figure 5c,d. Comparatively, the capacity of ASSLBs with $Li_{10}GeP_2S_{12}$ as electrolyte at approximately 1.27 mA cm$^{-2}$ is near 0 presented in Ref. [7a]. Furthermore, ASSLBs with thick electrode configurations were also evaluated (Figure 5e,f). Three ASSLBs with NMC811 loadings of 19.1, 44.59, and 89.17 mg cm$^{-2}$ were assembled, with reversible areal capacity of 2.64, 5.85, and 12.16 mAh cm$^{-2}$. The corresponding initial Coulombic Efficiency is 78.8%, 74.9% and 72.2%, which is comparable to reported NMC811 with much lower areal capacity ASSLBs. The well overlapped In $L_3$-edge and Cl K-edge XANES spectra of $Li_3InCl_6$ SSE at different charge/discharge status presented in Figure S24 proves the stability of $Li_3InCl_6$ SSE with NMC811 during cycling. The high interfacial stability of $Li_3InCl_6$/NMC811 was further reflected from the impedance evolution of the cell during charge/discharge process (Figure S25). Moreover, even the ASSLB with reheated $Li_3InCl_6$ as the electrolyte or Li metal as the anode can exhibit stable cycling (Figure S26,27). The results demonstrate that $Li_3InCl_6$ is applicable as a practical electrolyte for ASSLBs. Most importantly, the $H_2O$-mediated synthesis route can be also extended to prepare other ionic conductors such as $Na_3InCl_6$ (Figure S28).

In summary, halide-based $Li^+$-ion superionic conductor, $Li_3InCl_6$, is prepared by a facile and scalable $H_2O$-mediated synthesis route, which can be highly favorable for practical manufacturing. A high $Li^+$-ion conductivity of $2.04 \times 10^{-3}$ S cm$^{-1}$ is achieved at 25 °C. The reversible conversion between $Li_3InCl_6$ and $Li_3InCl_6{\cdot}2H_2O$ enables its intrinsic stability against air and humidity, thus ensuring high ionic conductivity is recovered after conversion. Meanwhile, $Li_3InCl_6$ is chemically and electrochemically stable in direct contact with high voltage oxide cath-

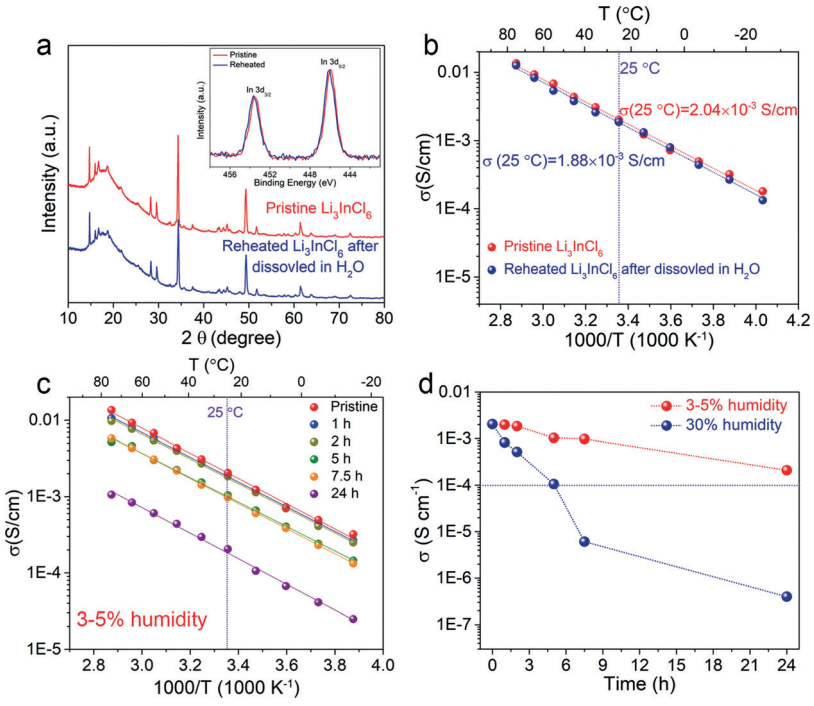


***Figure 4.*** Evaluation of $Li_3InCl_6$ stability in a humid environment. a) XRD patterns (Inset: In 3d XPS spectra) and b) ionic conductivities of the pristine $Li_3InCl_6$ SSE (red) and a sample completely dissolved in water and subsequently dried at 200 °C for 1 h under vacuum (blue). c) Arrhenius plots of $Li_3InCl_6$ SSE exposed in 3–5% humidity environment at different times. d) Ionic conductivity evolution of $Li_3InCl_6$ SSE exposed in 3–5% and 30% humidity environments at different times.

  

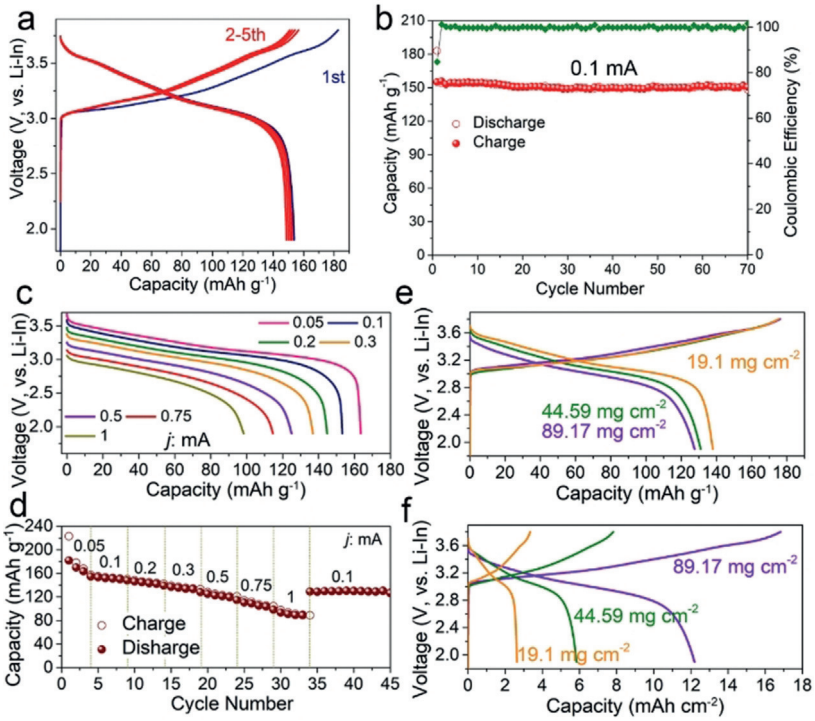


***Figure 5.*** Electrochemical performance of NMC811/$Li_3InCl_6$/$Li_{10}GeP_2S_{12}$/In all-solid-state cells at 25 °C. a) Charge–discharge curves and b) cycling performance of NMC811/$Li_3InCl_6$/$Li_{10}GeP_2S_{12}$/In cell at 0.1 mA. c),d) Rate capability of NMC811/$Li_3InCl_6$/$Li_{10}GeP_2S_{12}$/In cells at 0.05, 0.1, 0.2, 0.3, 0.5, 0.75, and 1 mA. e),f) Charge–discharge curve of high loading cells. Diameter of the electrode is 10 mm.

ode materials (e.g. NMC811). Good performance is demonstrated for ASSLBs using $Li_3InCl_6$ SSE with NMC811 cathode. Our results suggest that $Li_3InCl_6$ is a highly promising SSE candidate for practical ASSLBs and sustainable energy storage.

## Acknowledgements

This research was supported by Natural Sciences and Engineering Research Council of Canada (NSERC), GLABAT Solid-State Battery Inc., China Automotive Battery Research Institute Co. Ltd, Canada Research Chair Program (CRC), Canada Foundation for Innovation (CFI), Ontario Research Fund, the Canada Light Source at University of Saskatchewan (CLS), Canada MITACS fellow, and University of Western Ontario.

## Conflict of interest

The authors declare no conflict of interest.

**Keywords:** all-solid-state battery · aqueous synthesis · halide solid electrolyte · ionic conductivity · lithium

**How to cite:** *Angew. Chem. Int. Ed.* **2019**, *58*, 16427–16432
*Angew. Chem.* **2019**, *131*, 16579–16584

[1] a) Y. Kato, S. Hori, T. Saito, K. Suzuki, M. Hirayama, A. Mitsui, M. Yonemura, H. Iba, R. Kanno, *Nat. Energy* **2016**, *1*, 16030; b) Y. Ding, Z. P. Cano, A. Yu, J. Lu, Z. Chen, *Electrochem. Energy Rev.* **2019**, *2*, 1–28; c) M. A. Kraft, S. Ohno, T. Zinkevich, R. Koerver, S. P. Culver, T. Fuchs, A. Senyshyn, S. Indris, B. J. Morgan, W. G. Zeier, *J. Am. Chem. Soc.* **2018**, *140*, 16330–16339; d) J. C. Bachman, S. Muy, A. Grimaud, H.-H. Chang, N. Pour, S. F. Lux, O. Paschos, F. Maglia, S. Lupart, P. Lamp, *Chem. Rev.* **2016**, *116*, 140–162.

[2] a) N. Kamaya, K. Homma, Y. Yamakawa, M. Hirayama, R. Kanno, M. Yonemura, T. Kamiyama, Y. Kato, S. Hama, K. Kawamoto, A. Mitsui, *Nat. Mater.* **2011**, *10*, 682; b) L. Nazar, P. Adeli, J. D. Bazak, K.-H. Park, I. Kochetkov, A. Huq, G. Goward, *Angew. Chem. Int. Ed.* **2019**, *58*, 8681–8686; *Angew. Chem.* **2019**, *131*, 8773–8778; c) Y. Sun, K. Suzuki, S. Hori, M. Hirayama, R. Kanno, *Chem. Mater.* **2017**, *29*, 5858–5864.

[3] Z. Zhang, Y. Shao, B. Lotsch, Y.-S. Hu, H. Li, J. Janek, L. F. Nazar, C.-W. Nan, J. Maier, M. Armand, *Energy Environ. Sci.* **2018**, *11*, 1945–1976.

[4] a) X. Han, Y. Gong, K. K. Fu, X. He, G. T. Hitz, J. Dai, A. Pearse, B. Liu, H. Wang, G. Rubloff, *Nat. Mater.* **2017**, *16*, 572; b) M. Kotobuki, H. Munakata, K. Kanamura, Y. Sato, T. Yoshida, *J. Electrochem. Soc.* **2010**, *157*, A1076–A1079.

[5] a) H. Muramatsu, A. Hayashi, T. Ohtomo, S. Hama, M. Tatsumisago, *Solid State Ionics* **2011**, *182*, 116–119; b) T. Ohtomo, A. Hayashi, M. Tatsumisago, K. Kawamoto, *J. Mater. Sci.* **2013**, *48*, 4137–4142.

[6] a) J. Auvergniot, A. Cassel, J.-B. Ledeuil, V. Viallet, V. Seznec, R. m. Dedryvère, *Chem. Mater.* **2017**, *29*, 3883–3890; b) W. Zhang, D. A. Weber, H. Weigand, T. Arlt, I. Manke, D. Schröder, R. Koerver, T. Leichtweiss, P. Hartmann, W. G. Zeier, *ACS Appl. Mater. Interfaces* **2017**, *9*, 17835–17845; c) S. P. Culver, R. Koerver, W. G. Zeier, J. Janek, *Adv. Energy Mater.* **2019**, *9*, 1900626.

[7] a) R. Koerver, I. Aygün, T. Leichtweiß, C. Dietrich, W. Zhang, J. O. Binder, P. Hartmann, W. G. Zeier, J. r. Janek, *Chem. Mater.* **2017**, *29*, 5574–5582; b) H. Visbal, Y. Aihara, S. Ito, T. Watanabe, Y. Park, S. Doo, *J. Power Sources* **2016**, *314*, 85–92; c) G. Oh, M. Hirayama, O. Kwon, K. Suzuki, R. Kanno, *Chem. Mater.* **2016**, *28*, 2634–2640.

[8] Y. J. Nam, D. Y. Oh, S. H. Jung, Y. S. Jung, *J. Power Sources* **2018**, *375*, 93–101.

[9] a) H. J. Steiner, H. Lutz, *Z. Anorg. Allg. Chem.* **1992**, *613*, 26–30; b) W. Schmidt, H. Lutz, *Ber. Bunsen-Ges.* **1984**, *88*, 720–723; c) R. Kanno, Y. Takeda, M. Mori, O. Yamamoto, *Chem. Lett.* **1987**, *16*, 1465–1468; d) W. Weppner, R. Huggins, *J. Electrochem. Soc.* **1977**, *124*, 35–38.

[10] A. Manthiram, X. Yu, S. Wang, *Nat. Rev. Mater.* **2017**, *2*, 16103.

[11] a) K. Yamada, K. Iwaki, T. Okuda, Y. Tomita, in *Solid State Ionics: Trends in the New Millennium*, World Scientific, Singapore, **2002**, pp. 621–628; b) Y. Tomita, H. Nishiyama, K. Kobayashi, Y. Kohno, Y. Maeda, K. Yamada, *ECS Trans.* **2009**, *16*, 137–141.

[12] T. Asano, A. Sakai, S. Ouchi, M. Sakaida, A. Miyazaki, S. Hasegawa, *Adv. Mater.* **2018**, *30*, 1803075.

  

[13] R. Nagel, T. W. Groß, H. Günther, H. Lutz, *J. Solid State Chem.* **2002**, *165*, 303 – 311.
[14] L. Zhou, J.-F. Liao, Z.-G. Huang, J.-H. Wei, X.-D. Wang, W.-G. Li, H.-Y. Chen, D.-B. Kuang, C.-Y. Su, *Angew. Chem. Int. Ed.* **2019**, *58*, 5277 – 5281; *Angew. Chem.* **2019**, *131*, 5331 – 5335.
[15] O. Knop, T. S. Cameron, D. Adhikesavalu, B. R. Vincent, J. A. Jenkins, *Can. J. Chem.* **1987**, *65*, 1527 – 1556.
[16] Y. Tomita, H. Matsushita, H. Yonekura, Y. Yamauchi, K. Yamada, K. Kobayashi, *Solid State Ionics* **2004**, *174*, 35 – 39.
[17] X. Li, J. Liang, X. Li, C. Wang, J. Luo, R. Li, X. Sun, *Energy Environ. Sci.* **2018**, *11*, 2828 – 2832.
[18] F. Han, A. S. Westover, J. Yue, X. Fan, F. Wang, M. Chi, D. N. Leonard, N. J. Dudney, H. Wang, C. Wang, *Nat. Energy* **2019**, *4*, 187 – 196.
[19] S. Wang, Q. Bai, A. M. Nolan, Y. Liu, S. Gong, Q. Sun, Y. Mo, *Angew. Chem. Int. Ed.* **2019**, *58*, 8039 – 8043; *Angew. Chem.* **2019**, *131*, 8123 – 8127.
[20] a) J. Rodríguez-Carvajal, *Phys. B* **1993**, *192*, 55 – 69; b) V. Favre-Nicolin, R. Černý, *J. Appl. Crystallogr.* **2002**, *35*, 734 – 743; c) S. J. Clark, M. D. Segall, C. J. Pickard, P. J. Hasnip, M. I. Probert, K. Refson, M. C. Payne, *Z. Kristallogr. - Cryst. Mater.* **2005**, *220*, 567 – 570.
[21] N. Adelstein, B. C. Wood, *Chem. Mater.* **2016**, *28*, 7218 – 7231.
[22] J. J. Rehr, R. C. Albers, *Rev. Mod. Phys.* **2000**, *72*, 621.
[23] F. Strauss, T. Bartsch, L. de Biasi, A.-Y. Kim, J. r. Janek, P. Hartmann, T. Brezesinski, *ACS Energy Lett.* **2018**, *3*, 992 – 996.

Manuscript received: August 2, 2019
Accepted manuscript online: September 2, 2019
Version of record online: September 30, 2019

  